Interplay between interstitial and substitutional hydrogen donors in ZnO

S. G. Koch,* E. V. Lavrov,† and J. Weber
Technische Universität Dresden, 01062 Dresden, Germany
(Received 12 February 2014; revised manuscript received 6 June 2014; published 18 June 2014)

A Raman study on hydrogen donors in ZnO reveals the properties of bond-centered hydrogen (H_{BC}) and hydrogen trapped in the oxygen vacancy (H_O). The donors are identified by their electronic $1s \rightarrow 2s(2p)$ transitions and their characteristic local vibrational modes. The H_O donor was detected preferentially below the sample surface, where a high oxygen vacancy concentration is generated by thermal treatment of the samples. H_{BC} and H_O exhibit different thermal stabilities and their concentrations depend strongly on the sample history. Molecular hydrogen is an essential part of the interplay of the two hydrogen donors.

DOI: 10.1103/PhysRevB.89.235203 PACS number(s): 61.72.J−, 63.20.Pw, 71.55.Gs, 78.30.Fs

I. INTRODUCTION

Hydrogen is an inherent impurity in ZnO which strongly affects the electrical properties of this wide-band-gap semiconductor [1,2]. Both interstitial and substitutional species act as shallow donors [3–5]. The interstitial hydrogen is bond-centered (H_{BC}) with a strong O–H bond resulting in a local vibrational mode (LVM) at 3611 cm^{-1} [6,7]. Hydrogen substituting for O binds nearly equally to all four Zn atoms [8], which results in two LVMs at 742 and 792 cm^{-1} originating from the A_1 and E representations of the C_{3v} point group [9].

The ionization energies of the H_{BC} and H_O shallow donors are 53 and 47 meV, respectively [7,10,11]. Photoconductivity (PC) and photoluminescence (PL) measurements reveal the $1s \rightarrow 2p$ electronic transitions to be at 330 (H_{BC}) and 265 cm^{-1} (H_O). These transitions were also found in Raman spectra of ZnO (see Ref. [12]), albeit the Raman line of the H_O donor was blue-shifted compared to the PL and PC measurements making the assignment somewhat ambiguous.

Since both H_{BC} and H_O contain the same impurity, the nature of the dominant hydrogen donor species in ZnO samples should depend on the growth conditions, sample history, and the details of sample processing. Experimental results indicate that directly after hydrogenation of a bulk sample or growth of a ZnO thin film, the bond-centered species is the dominant donor. On the other hand, theoretical investigations of the formation energies yield the H_O complex to be energetically more favorable [8,13].

The annealing temperature of H_{BC} depends on the amount of other hydrogen trapping centers and in pure material is determined solely by the formation rate of hydrogen molecules [14,15]. For concentrations of bond-centered hydrogen at 10^{17} cm^{-3}, the annealing temperature was reported to be around 200 °C [7,16,17]. Substitutional hydrogen is significantly more stable and depending on the sample history anneals out at temperatures between 650 °C and 800 °C [11].

Most of the experimental information about the properties of H_O was obtained from photoconductivity and photoluminescence studies which are restricted to a near-surface layer of ZnO. The local inhomogeneities result from the nonuniform oxygen vacancy distribution created by high-temperature treatments. A direct comparison between the formation of the two donors is not possible and hinders a support of calculations.

Here, we present the results of a Raman study, which focuses on the interplay between the two main hydrogen donors in ZnO. This measurement technique is not limited to the near-surface layer but extends across the whole sample, thus providing a detailed insight into the properties of H_{BC} and H_O.

II. EXPERIMENT

The samples in this study were nominally undoped vapor phase grown ZnO single crystals grown in the Institute for Applied Physics, University of Erlangen (Germany) [18,19]. Hydrogen and/or deuterium was incorporated into the samples via thermal treatment at temperatures of 1000 °C for 1 h in sealed quartz ampoules filled with H_2 and/or D_2 gas (pressure of 0.5 bar at room temperature). This process was terminated by quenching the samples to room temperature in water. Directly after hydrogenation, the samples exhibited a gray surface. A shiny surface was created by removing about 50–150 μm from each face by mechanical polishing. Subsequent annealing steps were performed in Ar atmosphere for 0.5–1 h in the temperature range 100 °C–1000 °C.

The Raman measurements were conducted in a 90° geometry using the frequency-doubled 532-nm line of a Nd:YVO_4 laser with a power of 1 W for excitation in the temperature range 49–296 K. The scattered light was analyzed using a monochromator (Czerny-Turner arrangement) and a liquid-nitrogen-cooled Si CCD detector array. The spectral resolution was 2.5–3.6 cm^{-1}. The integration time was dependent on the spectral region and ranged from 1 min for the phonon spectrum of ZnO to 2 h for the hydrogen-related vibrational modes. To account for misalignments in the sample mounting, Raman spectra were calibrated with respect to the intensity and frequency of the A_1(TO) phonon mode at 380 cm^{-1}.

The scattering geometry is defined in the coordinate system of the sample, with the x, y, and z axes parallel to the $[10\bar{1}0]$, $[1\bar{2}10]$, and c axes, respectively. If not noted otherwise, the $x(z,-)y$ configuration was used [20]. The notation "−" implies that no polarizer was employed to analyze the scattered light. Depth profile measurements were carried out via shifting the sample along the y axis and recording Raman spectra as a function of shift. The laser excitation volume was focused on

*sandro.koch@physik.tu-dresden.de
†Also at Institute of Radioengineering and Electronics, Mokhovaya 11, 101999 Moscow, Russia.

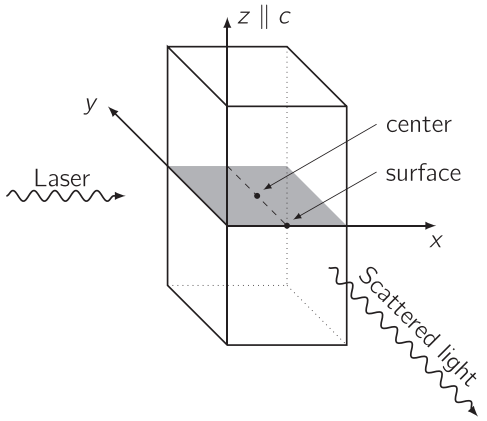

FIG. 1. Sketch of the Raman scattering geometry employed in this study. Depth profile measurements were performed along the dashed line. The scattering position in the middle of the sample and at the surface are labeled "center" and "surface," respectively.

the dashed line (see Fig. 1). It had a shape of a cylinder with the axis parallel to x and a diameter of about 35 μm. A mask placed on the xz face of the sample was used to filter off the light reflected from the side faces.

Infrared absorption measurements were carried out with a Bomem DA3.01 Fourier transform spectrometer equipped with a CaF_2 beamsplitter, a globar light source, and a liquid-nitrogen-cooled InSb detector. The spectral resolution was 0.25–0.50 cm^{-1}. Measurements were performed in a He exchange-gas cryostat equipped with ZnSe windows.

Photoluminescence (PL) measurements were performed with the sample immersed in liquid He (4.2 K). The 325-nm line of a HeCd laser with a typical power of 3 mW was used for excitation. The emitted light was analyzed by a SPEX monochromator equipped with a 1200 grooves/mm grating and detected by a Peltier-cooled photomultiplier (RCA C31034). The spectral resolution was 0.084 nm.

III. IMPACT OF HIGH-TEMPERATURE TREATMENTS ON H_{BC}

A. Electronic transition of H_{BC}

Figure 2 presents low-temperature Raman spectra taken from the "center" of a ZnO sample before and directly after hydrogenation in a mixture of H_2 and D_2 at 1000 °C. The treatment results in the formation of H_{BC} and D_{BC} which manifest themselves as the $1s \rightarrow 2s(2p)$ donor transition(s) at 340 cm^{-1} and the local vibration modes due to H_{BC} and D_{BC} at 3611 and 2668 cm^{-1}, respectively [7]. Additionally, the E_1(LO) phonon line changes in intensity and shape due to the Fano interaction with the continuum of the electronic H_{BC} (D_{BC}) shallow donor states. We note that the electronic $1s \rightarrow 2s(2p)$ transition is blue-shifted by about 7 cm^{-1} compared to the values obtained after hydrogenation at 725 °C [7].

Figure 3 presents Raman spectra recorded for ZnO samples after hydrogenation with H_2, D_2, and $H_2 + D_2$. As expected, no detectable isotope effect on the electronic $1s \rightarrow 2s(2p)$ transition(s) of the bond-centered hydrogen can be seen.

Table I lists frequencies of the electronic donor transitions due to H_{BC} together with its concentration and the

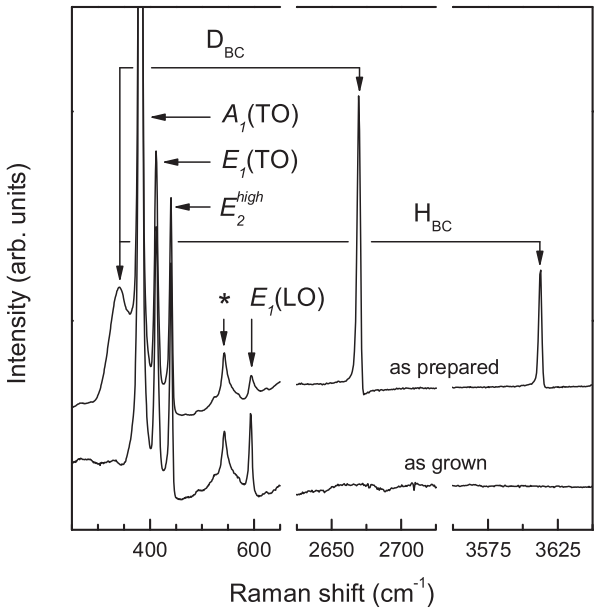

FIG. 2. Raman spectra taken in the "center" of a ZnO sample before (bottom) and directly after (top) hydrogenation in a mixture of deuterium and hydrogen at 1000 °C. The feature labeled with "∗" is assigned to a multiphonon mode [20–22]. The spectra were recorded at $T \leqslant 55$ K.

hydrogenation temperature (T_H) of ZnO sample grown under the same conditions. The $1s \rightarrow 2s(2p)$ transition(s) revealed in the Raman spectra of the samples treated at 1000 °C is(are) always blue-shifted by about 7 cm^{-1} compared to the values obtained via photoluminescence, photoconductivity, and Raman measurements after hydrogenation at 725 °C (see Ref. [7]) but matches the Raman value reported after

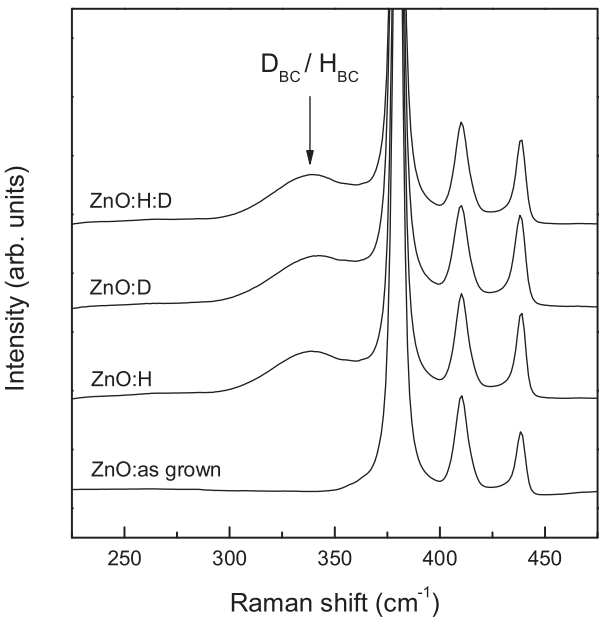

FIG. 3. Raman spectra taken in the center of ZnO samples treated with different hydrogen isotopes and isotope mixture at 1000 °C. The spectra were recorded at $T \leqslant 55$ K.

TABLE I. Frequencies of the electronic shallow donor transition of H_{BC} and/or D_{BC} in ZnO hydrogenated under different conditions. The concentration was determined using Eq. (3) in Ref. [7].

T_H (°C)	species X	N_X (cm^{-3})	$1s \rightarrow 2s(2p)$ (cm^{-1})	Ref.
725	H_{BC}	1.5×10^{17}	333	[7]
1000	H_{BC}	$\leqslant 4 \times 10^{18}$	341	[12]
1000	H_{BC}	5×10^{17}	340 ± 1	This study
1000	D_{BC}	$\geqslant 3 \times 10^{17}$	342 ± 1	This study
1000	H_{BC},D_{BC}	3×10^{17}	340 ± 1	This study

hydrogenation at 1000 °C (see Ref. [12]). Under conditions employed in this study, the solubility limit of hydrogen in ZnO is 3×10^{18} cm^{-3} [2]. Since H_{BC} is the dominant donor with a concentration close to the solubility limit of hydrogen, the free carrier concentration at $T \leqslant 55$ K can be estimated to be below 3×10^{15} cm^{-3} [23]. The energy of the electronic transition(s) as well as the concentration of H_{BC} are changed by the details of the treatment but the LVM frequency of H_{BC} remains unchanged.

We consider the following possibilities for the blue-shift of the $1s \rightarrow 2s(2p)$ transition(s):

(i) In polar semiconductors, the Coulomb interaction between infrared-active lattice vibrations and the free carriers leads to a coupling of the LO phonons and the plasmon vibrations [24]. With the parameters of ZnO known from the literature (see Ref. [25]), the free-carrier concentration necessary for a resonance interaction with the electronic transition is determined to be three orders of magnitude above the experimental value, which rules out the polariton-plasmon mechanism as a possible reason of the energy shift.

(ii) From Table I one can see that the blue-shift of the $1s \rightarrow 2s(2p)$ transition(s) seems to be proportional to the hydrogen concentration. The solubility limit of hydrogen at our treatment temperature fulfills almost the Mott criterion [26] in ZnO indicating an interaction between the donor states. As mentioned already, the majority of the H_{BC} shallow donors during the measurements are in the neutral charge state. In this case, the resonant dipole-dipole interaction is dominant, but should result in a *red-shift* and a broadening of the electronic transitions of shallow donors [27]. The expansion of the donor electron wave functions scales with the square of the main quantum number n. Hence, the overlap of the wave functions and thus a donor level band broadening occur at lower impurity concentration for the $n = 2$ states compared to the $n = 1$ state [28]. However, the line position and shape of the $1s \rightarrow 2s(2p)$ transition do not only depend on the splitting of the donor bands, but also on the density of states within these bands making a general prediction challenging. To the best of our knowledge, only a red-shift was experimentally established, e.g., in Si [29] and in Ge [30]. Therefore, the overlap of the wave functions due to bound electrons is unlikely but can not be ruled out as a cause for the blue-shift of the $1s \rightarrow 2s(2p)$ transition(s) of H_{BC}.

(iii) Additionally to the shallow donors, our ZnO samples could contain acceptors. The random electric fields of the ionized acceptors (e.g., Zn vacancies) will affect the shallow donor states. Still, the interaction with charged defects should result in a *red-shift* of the electronic transitions and can not therefore account for the experimental observations [31].

(iv) Table I also indicates that the blue-shift of the $1s \rightarrow 2s(2p)$ transition(s) depends on the temperature of the hydrogenation. Indeed, the treatment at 1000 °C makes the sample surface gray and milky, which does not take place for temperatures below 750 °C. This strongly indicates that the high-temperature treatment causes considerable lattice damages possibly related to the agglomerates of native defects such as vacancies and/or interstitials.

The effect of hydrostatic and uniaxial stress on the phonon modes in ZnO at room temperature was investigated earlier [32]. In order to compare these results with our findings, room-temperature Raman measurements for the samples hydrogenated in the temperature range 800 °C to 1000 °C were carried out. No noticeable shift relative to the virgin sample was detected for the A_1(TO), E_1(TO), and E_2^{high} phonon modes. We take this as an indication that the hydrogenation-induced strain results in a local rather than extended lattice distortion affecting the hydrogen donor states. Recent findings on the LVM shift of the H_2 molecules in ZnO support this model (see Sec. IV C) [33].

B. Temperature dependence of the H_{BC} LVM

The temperature dependence of the LVM frequency of H_{BC} is presented in Fig. 4(a). As the temperature rises, the line red-shifts and broadens. Such a behavior is often explained by a dephasing of the LVM due to an anharmonic interaction with the lattice vibrations whereas the number of the involved phonons play a crucial role. Harris *et al.* [34] and Persson and Ryberg [35] consider an interaction with a single low-energy phonon. Lüpke *et al.* [36] and Martin *et al.* [37] developed a theory for more than one exchange mode. The involvement of other LVMs into the dephasing process was considered

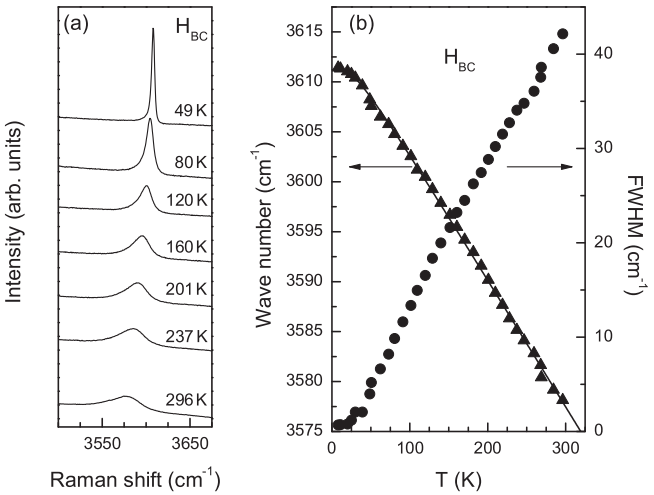

FIG. 4. Temperature dependence of the H_{BC} LVM frequency. (a) Raman spectra recorded in the temperature range 49 K to room temperature. (b) The frequency at peak maximum (filled triangle) and the FWHM (filled circle) determined from a Pearson IV fit are plotted over the sample temperature. The values for temperatures below 50 K originate from previous IR measurements (see Ref. [6]).

by West and Estreicher [38]. The model by McCumber and Sturge [39] and Elliott *et al.* [40] includes acoustical rather than optical phonons in the process.

Coupling with only acoustical phonons would not fit our experimental data. We apply therefore the model proposed by Persson and Ryberg which was later modified for the zero-energy contribution [41]. The model takes into account an interaction between a LVM anharmonically coupled to a single exchange mode E_0 through a parameter $\delta\sigma$. The exchange mode is in turn anharmonically coupled to the phonon bath through a "friction" parameter η. Note that this approach is valid only in the limit of $\delta\sigma/\eta \ll 1$. The exchange mode could be a phonon as well as another stretch, wag, or rotational mode of the defect. The position and the width of the LVM are expressed by

$$\sigma(T) = \sigma_0 + \frac{\delta\sigma}{\exp(E_0/k_BT) - 1}, \quad (1)$$

$$\Delta\Gamma(T) = \frac{2(\delta\sigma)^2}{\eta}\left(\frac{1}{2} + \frac{1}{\exp(E_0/k_BT) - 1}\right)^2. \quad (2)$$

Within this model, the "best-fit" parameters for the H_{BC} LVM using Eq. (1) are

$$\sigma_0 = 3611.2 \pm 0.4\ \text{cm}^{-1},$$
$$\delta\sigma = -9.4 \pm 1.7\ \text{cm}^{-1},$$
$$E_0 = 51.3 \pm 8.3\ \text{cm}^{-1}.$$

The corresponding fitting curve depicted as solid line in Fig. 4(b) matches the LVM frequency of H_{BC} reasonably well over the whole temperature range. Within the error bars, the observed exchange mode E_0 is slightly below the values determined from the hydrogen motion in the Li–OH and CuH_2 complexes [37,42].

In order to justify the applicability of the model by Persson and Ryberg, the estimation of the "friction" parameter η is necessary. A reasonable fit of the linewidth $\Delta\Gamma(T)$ using Eq. (2) was not possible since the lineshape is strongly asymmetric. However, from the experimentally obtained linewidth at low temperatures $\Delta\Gamma \approx 0.7\ \text{cm}^{-1}$ and Eq. (2) we obtain that $\eta > 63.1\ \text{cm}^{-1}$ and hence the above-mentioned weak-coupling condition ($|\delta\sigma/\eta| = 0.15 \pm 0.03 \ll 1$) is well fulfilled [43].

A Pearson IV distribution rather than natural lineshape was employed to present the data in Fig. 4(b). Presumably, the asymmetry of the LVM is caused by the Fano resonance with the energy spectrum of electrons in the conduction band. Based on this, we expect that the peak position plotted in Fig. 4(b) is red-shifted compared to the "pure" LVM. The absolute difference between these values $\Delta\sigma$ is proportional to the product of the linewidth of the unperturbed LVM and the inverse Fano parameter $1/q$ [44]. Since the "pure" LVM is expected to experience at least a thermal broadening the shift $\Delta\sigma$ increases with temperature. This results in an underestimation of E_0 in our "best-fit" parameters of Eq. (1) and accounts for the deviation from the values reported in Refs. [37,42]. Note that the linewidth in the case of Fano resonance is a combined effect of the "friction" with the lattice as well as the interaction with the electron continuum, which prevented us from a more detailed analysis of $\Delta\Gamma$.

IV. INTERPLAY BETWEEN H_{BC} and H_O

A. Concentration profile of H_{BC}

Figure 5(a) presents Raman spectra of a ZnO sample hydrogenated at 1000 °C. The spectra were recorded for different excitation spots along the y axis (see Fig. 1). Since interstitial hydrogen is a fast diffusing species [7,15–17], the electronic transition at 340 cm^{-1} and the LVM at 3611 cm^{-1} of H_{BC} can be detected across the whole sample. Towards

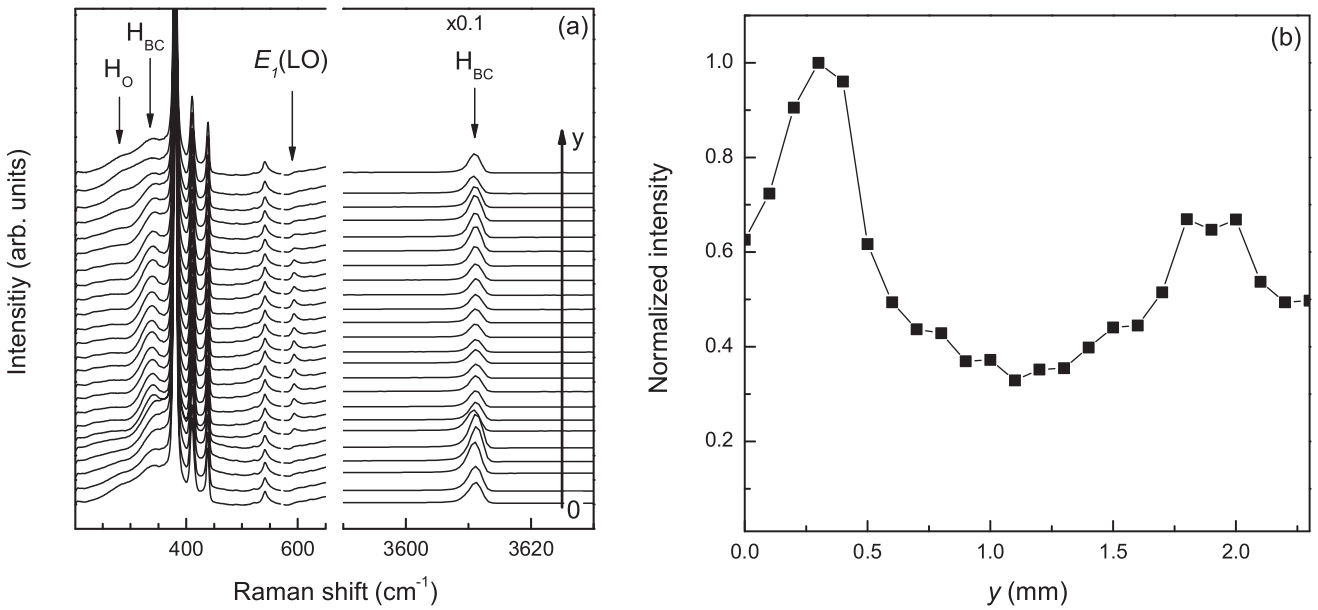

FIG. 5. Depth profiles obtained for a ZnO sample hydrogenated at 1000 °C. (a) Raman spectra as a function of y normalized to the intensity of the A_1(TO) phonon. The bottom and top spectra were recorded on the front side and the back side of the sample with respect to the entrance slit of the monochromator, respectively (see Fig. 1). (b) Normalized intensity of the LVM of H_{BC} at 3611 cm^{-1}.

the sample surface the $1s \rightarrow 2s(2p)$ donor transition of H_{BC} significantly broadens but only marginally blue-shifts due to the lattice damage induced by the heat treatment. The intensity of the E_1(LO) phonon line at about 590 cm^{-1} anticorrelates with the H_{BC} signals. This behavior was explained earlier by a Fano resonance between the phonon mode and the continuum of electronic states in the conduction band [7].

Photoluminescence measurements on two ZnO samples hydrogenated at 750 °C and 1000 °C were performed in order to verify the observed Raman shift in the electronic transition of H_{BC}. The near-band-edge signals, that are detectable within the penetration depth of about 50 nm, experienced a significant broadening due to the surface damage. Additionally, the donor-bound exciton (D^0X) recombination and two-electron satellite (TES) transitions of H_{BC} are known to overlap with the I_{6a} and I_7 related lines [7]. Only for the sample annealed at 1000 °C a TES signal in the expected region of H_{BC} is visible. The PL data reveal a $1s \rightarrow 2s(2p)$ donor transition for H_{BC} at 334 ± 7 cm^{-1} with a broad shoulder at the high-energy side preventing us from a definitive confirmation of the blue-shift. In both samples, the I_4 related lines associated with H_O were detected, which exhibit a shallow donor transition of about 266 cm^{-1}. This value matches the $1s \rightarrow 2p$ transition as reported previously (see Ref. [7]) confirming the presence of H_O directly after the hydrogenation.

B. Identification of the shallow donor transition of H_O

Additionally, a weak shoulder at around 283 cm^{-1} appears in Fig. 5(a) for the excitation spots at the sample surface. Lines close to this value have been assigned in the literature to (i) the LVM of the $Zn_i - N_O$ complex [50–55], (ii) silent B modes of ZnO [21,22,46–49], and (iii) the $1s \rightarrow 2s(2p)$ donor transition of H_O [7,10–12].

(i) The assignment of the 283-cm^{-1} line to $Zn_i - N_O$ should be rejected since our samples did not receive a nitrogen treatment. Besides, the vibrational mode of this complex was found to be significantly narrower and has a frequency of 275 cm^{-1}.

(ii) Wurtzite ZnO belongs to the C_{6V}^4 space group. The nine optical phonons in the center of the Brillouin zone are transformed as the following irreducible representation of the C_{6V}^4 point group: $A_1 + 2B_1 + E_1 + 2E_2$ [56]. Of these, the two B_1 modes (B_1^{low} and B_1^{high}) are silent and can not be seen in Raman scattering. The situation changes when the translational invariance is broken as it happens in the case of the temperature-induced damage.

Table II summarizes frequencies of the B_1 modes reported in the literature. Two features at about 270 and 550 cm^{-1} are supposed to appear as a result of high-temperature treatment. On the other hand, only one mode at around 283 cm^{-1} occurs in our spectra based on which we exclude the silent modes as an origin for this transition.

(iii) The high-temperature treatment leads to a formation of oxygen vacancies (V_O) in the near-surface layer of a sample. The passivation of vacancies with hydrogen is energetically more favorable than the formation of H_{BC} [8,13]. Figure 5(b) shows the intensity of the 3611-cm^{-1} vibrational mode of H_{BC}. It has a maximum not directly at but close to the surface,

TABLE II. Calculated frequencies (cm^{-1}) of the silent B_1 phonons in ZnO.

B_1^{low}	B_1^{high}	Ref.
277		[21,45]
268	552	[22]
261	552	[46]
275	582	[47]
260	552	[48]
277	534	[49]

which we explain by the trapping of atomic hydrogen at the oxygen vacancies which are dominant defects directly at the sample surface. The reduction of the LVM intensity of H_{BC} anticorrelates with the intensity line at 283 cm^{-1}. The formation depth of H_O depends on the details of treatment (temperature, time, ambient) [57]. The net concentration of hydrogen donors is maximal near the sample surface leading to a significant broadening and finally to the disappearance of the E_1(LO) line. Based on these arguments, we assign the broad band at 283 cm^{-1} to the electronic $1s \rightarrow 2s(2p)$ transition of H_O. The observed blue-shift of this signal compared to the $1s \rightarrow 2p$ donor transition of H_O at 265 cm^{-1}, which was reported previously [7,10,11], agrees with the result of the bond-centered hydrogen (see Sec. III A) but needs to be analyzed in more detail.

Figure 6(a) presents normalized Raman spectra of the same ZnO sample as shown in Fig. 5 but after receiving a subsequent heat treatment at 200 °C. It is known that such a treatment results in the disappearance of the bond-centered hydrogen features from the Raman spectra [7].

The annealing at 200 °C also enhances the electronic $1s \rightarrow 2s(2p)$ transition of H_O at about 283 cm^{-1}. Furthermore, the E_1(LO) phonon line almost recovers its intensity and shape in the bulk of the sample since the total concentration of hydrogen-related shallow donors drops as a result of the annealing.

The intensity of the H_O follows the nonuniform concentration profile of the oxygen vacancies and has a maximum located at the sample surface. Unexpectedly, the frequency of the $1s \rightarrow 2s(2p)$ line blue-shifts towards the sample surface as shown in Fig. 6(b). From the figure we obtain a formation depth of H_O of about 280 μm. Note that extrapolation of the results presented in Ref. [57] to 1000 °C would give us the value of about 2 cm. We take this as an indication that the formation process of the oxygen vacancies is a function of many parameters, so that the comparison of the results obtained after annealing in different temperature regimes should be done with some care.

The inset in Fig. 6(b) shows the frequency of the electronic transition due to the H_O shallow donor versus its intensity. As the concentration goes to zero, its frequency approaches the value of 273.2 ± 0.3 cm^{-1}. Substitution of hydrogen with a mixture of hydrogen and deuterium yields the same formation depth and low-concentration frequency limit indicating that these properties are independent of the hydrogen isotope and are in fact a property of the ZnO lattice.

Recent photothermal ionization spectroscopy (PTIS, see Ref. [31]) studies have shown that the $1s \rightarrow 2p$ line of H_O

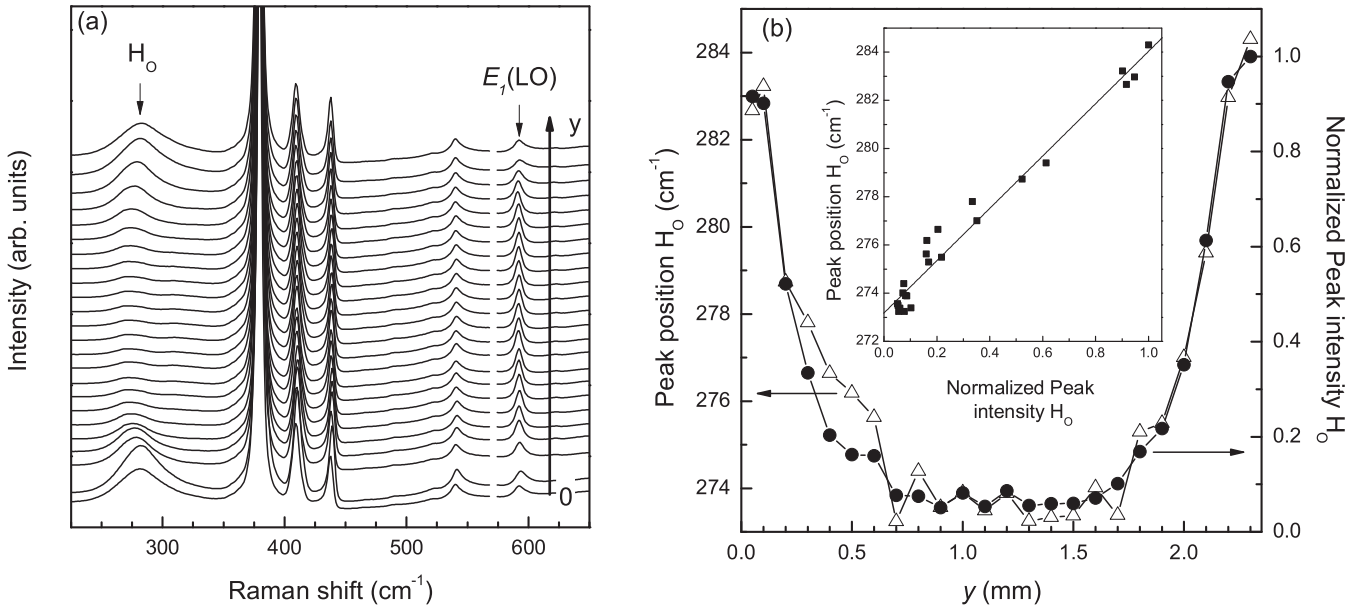

FIG. 6. Depth profiles obtained for a ZnO sample hydrogenated at 1000 °C after the annealing in Ar at 200 °C. (a) Raman spectra as a function of y normalized to the intensity of the A_1(TO) phonon. The bottom and top spectra were recorded on the front side and the back side of the sample with respect to the entrance slit of the monochromator, respectively. (b) Normalized intensity (filled circle) and position in the spectrum (open triangle) of the $1s \rightarrow 2p$ transition due to H_O. The normalized intensity of the $1s \rightarrow 2p$ transition vs peak position is presented in the inset. The solid line is a linear fit.

is split into two components with the frequencies of 262 and 267 cm^{-1} due to the $1s \rightarrow 2p_z$ and $1s \rightarrow 2p_{x,y}$ transitions, respectively [7]. The $1s \rightarrow 2s$ line can not be seen in PTIS, but is detected in photoluminescence spectra as a two-electron satellite of the main no-phonon recombination transition of the bound exciton [11]. From PL studies its frequency was found to be 272 cm^{-1}, which is very close to the value observed in the present Raman studies in the low-concentration limit. Polarized Raman spectra of the observed signal comply with the A_1 symmetry of the $2s$ state of a shallow donor in wurtzite ZnO (see Fig. 7). Based on these findings, we assign the 273-cm^{-1} line to the $1s \rightarrow 2s$ transition of H_O.

It follows also from Fig. 6(b) that the blue-shift of the $1s \rightarrow 2s$ band correlates with the amount of H_O and/or damages caused by the heat treatment. This significant increase of the shallow donors concentration towards the sample surface is directly mirrored by the intensity drop of the E_1(LO) phonon induced by the Fano resonance.

Note that recent NMR investigations have shown that at temperatures above 370 K, interstitial hydrogen becomes trapped at the oxygen vacancy with the energy gain of 0.51 eV [58], which gives us further support for the assignment of the 273 cm^{-1} line to the H_O donor.

C. Annealing properties of H_{BC} and H_O

Figure 8 presents Raman spectra of an isochronal annealing series of a ZnO sample that was treated in a mixture of D_2 and H_2. After annealing at 200 °C, the H_{BC} (D_{BC}) species disappears from the spectra and most of the oxygen vacancies are passivated by hydrogen.

Further annealing results in a reappearance of the H_{BC} (D_{BC}) signals in the bulk of the sample [see Fig. 8(a)] for the temperatures above 300 °C. A similar behavior was observed after annealing ZnO at 400 °C for the zinc vacancy passivated with one or two hydrogen atoms [6,14,59,60]. At 650 °C, bond-centered hydrogen (deuterium) reaches its maximum concentration but after annealing at 800 °C the defect is finally gone. The substitutional hydrogen (deuterium) is not affected

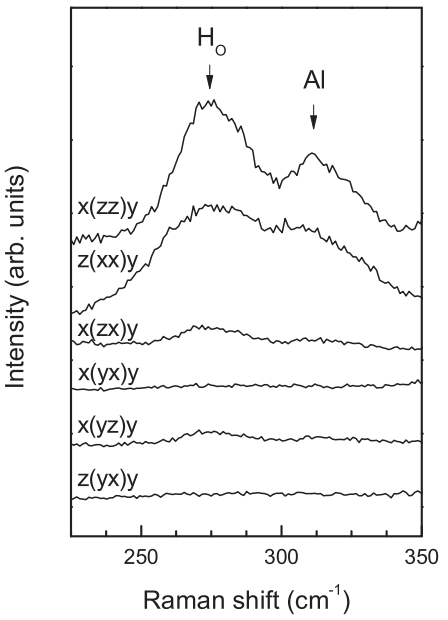

FIG. 7. Polarized Raman spectra of the $1s \rightarrow 2p$ transition due to H_O recorded at the center a ZnO sample.

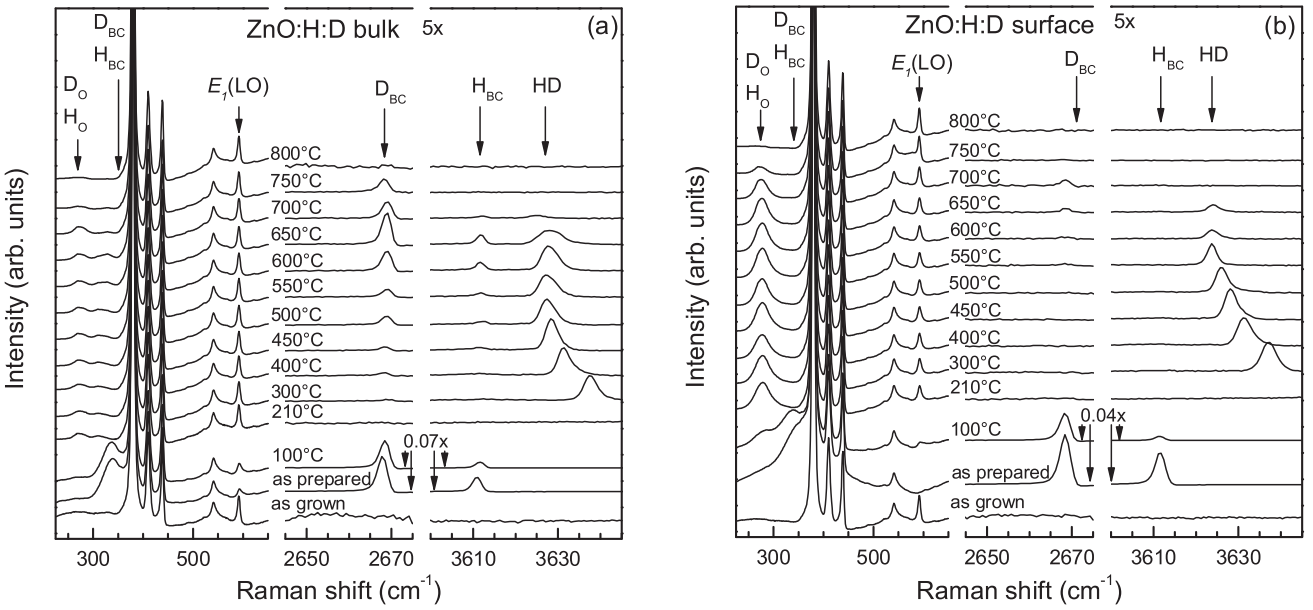

FIG. 8. Raman spectra of an isochronal annealing series of a ZnO sample treated in a mixture of hydrogen and deuterium taken in (a) the center and (b) surface position of the sample. The spectra were recorded at $T \leqslant 55$ K. The spectra in the LVM region are scaled by the depicted factor.

by these treatment steps until approximately 700 °C. It anneals out together with the bond-centered species at 800 °C.

At the sample surface [see Fig. 8(b)], the regeneration of the bond-centered species is less distinct. On the other hand, the H_O (D_O) features are much stronger than in the bulk. Both hydrogen donors anneal out at the same temperature of 800 °C as in the bulk of the sample.

We explain these findings as follows: First-principles theory predicts that H_{BC} is the ground state of hydrogen in ZnO for nearly all Fermi level energies except those close to the conduction band minimum [3]. Indeed, the 1000 °C treatment of the ZnO sample in hydrogen pushes the Fermi energy level deep into the band gap. This nonequilibrium state is preserved via quenching and hydrogen preferentially occupies the interstitial bond-centered site. The diffusion barrier of H_{BC} is low [16] so that hydrogen becomes mobile during annealing at elevated temperatures and will be trapped by all available oxygen vacancies forming H_O while moving around the crystal. However, the reappearance of the bond-centered hydrogen (deuterium) and the prolonged stability of the substitutional hydrogen stem from an unknown hydrogen source.

The formation of two hydrogen donors in concentrations above 10^{17} cm^{-3} ensures that the Fermi level is positioned at the bottom of the conduction band, which implies that isolated hydrogen should eventually convert into H_2 [3]. Indeed, at around 200 °C a broad line close to the frequency of HD grows in [see Figs. 8(a) and 8(b)]. With increasing annealing temperature, this signal red-shifts approaching the LVM frequency reported previously [61]. This finding confirms the theoretical predicted formation of the hydrogen molecule. A detailed analysis of the H_2 properties in ZnO is part of further investigations [33].

Hence, after annealing at 200 °C, all hydrogen in ZnO exists as interstitial H_2 and substitutional H_O species. The hydrogen molecule is, however, electrically inactive, which together with further increase of the annealing temperature pushes the Fermi level towards the middle of the band gap. This again makes H_{BC} energetically favorable compared to H_2, which results in a dissociation of the molecules and a reappearance of H_{BC}. This happens at temperatures above 300 °C.

After annealing at 650 °C–700 °C, the molecule is completely dissociated resulting in the maximum concentration of the bond-centered species. As the annealing temperature increases, hydrogen diffuses towards the sample surface and gradually leaves the sample. The intensity of H_O remains constant until the hydrogen supply from the bulk is over. Therefore, the apparent annealing temperature of substitutional hydrogen depends not only on its binding energy, but also on a number of experimental parameters including the thickness of the sample, which explains the differences in the literature about the annealing temperature.

V. SUMMARY

A Raman investigation of substitutional (H_O) and interstitial (H_{BC}) hydrogen in ZnO samples subjected to a high-temperature treatment is reported. It is shown that the induced lattice imperfections result in a blue-shift of the $1s \rightarrow 2s(2p)$ donor transition of H_{BC}. The $1s \rightarrow 2s$ transition energy of H_O is identified at 273 cm^{-1} and is found to scale with the H_O defect concentration. Analysis of the interplay of the two donors confirms earlier photoluminescence studies and theoretical conclusions indicating that H_O is energetically more preferable than H_{BC}. The influence of the hydrogen molecules is also discussed.

ACKNOWLEDGMENTS

This work was partially funded by the German Research Foundation (Grant No. LA 1397/4-1). F. Herklotz is acknowledged for fruitful discussions.

[1] E. Mollwo, Z. Phys. **138**, 478 (1954).
[2] D. G. Thomas and J. J. Lander, J. Chem. Phys. **25**, 1136 (1956).
[3] C. G. Van de Walle, Phys. Rev. Lett. **85**, 1012 (2000).
[4] S. Limpijumnong and S. B. Zhang, Appl. Phys. Lett. **86**, 151910 (2005).
[5] M. G. Wardle, J. P. Goss, and P. R. Briddon, Phys. Rev. B **72**, 155108 (2005).
[6] E. V. Lavrov, J. Weber, F. Börrnert, C. G. Van de Walle, and R. Helbig, Phys. Rev. B **66**, 165205 (2002).
[7] E. V. Lavrov, F. Herklotz, and J. Weber, Phys. Rev. B **79**, 165210 (2009).
[8] A. Janotti and C. G. Van de Walle, Nat. Mater. **6**, 44 (2007).
[9] S. G. Koch, E. V. Lavrov, and J. Weber, Phys. Rev. Lett. **108**, 165501 (2012).
[10] A. Schildknecht, R. Sauer, and K. Thonke, Phys. B (Amsterdam) **340–342**, 205 (2003).
[11] B. K. Meyer, H. Alves, D. M. Hofmann, W. Kriegseis, D. Forster, F. Bertram, J. Christen, A. Hoffmann, M. Straßburg, M. Dworzak, and U. Haboeck, Phys. Status Solidi B **241**, 231 (2004).
[12] E. V. Lavrov, Phys. B (Amsterdam) **404**, 5075 (2009).
[13] M.-H. Du and K. Biswas, Phys. Rev. Lett. **106**, 115502 (2011).
[14] F. Herklotz, E. V. Lavrov, Vl. Kolkovsky, J. Weber, and M. Stavola, Phys. Rev. B **82**, 115206 (2010).
[15] M. G. Wardle, J. P. Goss, and P. R. Briddon, Phys. Rev. Lett. **96**, 205504 (2006).
[16] F. Börrnert, E. V. Lavrov, and J. Weber, Phys. Rev. B **75**, 205202 (2007).
[17] K. M. Johansen, J. S. Christensen, E. V. Monakhov, A. Yu. Kuznetsov, and B. G. Svensson, Appl. Phys. Lett. **93**, 152109 (2008).
[18] G. Müller and R. Helbig, J. Phys. Chem. Solids **32**, 1971 (1971).
[19] R. Helbig, J. Cryst. Growth **15**, 25 (1972).
[20] T. C. Damen, S. P. S. Porto, and B. Tell, Phys. Rev. **142**, 570 (1966).
[21] J. M. Calleja and M. Cardona, Phys. Rev. B **16**, 3753 (1977).
[22] R. Cuscó, E. Alarcón-Lladó, J. Ibáñez, L. Artús, J. Jiménez, B. Wang, and M. J. Callahan, Phys. Rev. B **75**, 165202 (2007).
[23] K. Seeger, *Semiconductor Physics*, 9th ed. (Springer, Berlin, 2004).
[24] B. B. Varga, Phys. Rev. **137**, A1896 (1965).
[25] O. Madelung, *Semiconductors: Data Handbook*, 3rd ed. (Springer, Berlin, 2004).
[26] N. F. Mott, Rev. Mod. Phys. **40**, 677 (1968).
[27] L. D. Landau and E. M. Lifschitz, *Quantum Mechanics: Non-Relativistic Theory*, 3rd ed. (Pergamon, Oxford, England, 1977).
[28] W. Baltensperger, Philos. Mag. **44**, 1355 (1953).
[29] R. H. Kuwahara, Ph.D. thesis, University of British Columbia, Vancouver, Canada, 1971.
[30] A. Imatake, J. Phys. Soc. Jpn **35**, 164 (1973).
[31] S. M. Kogan and T. M. Lifshits, Phys. Status Solidi A **39**, 11 (1977).
[32] G. Callsen, J. S. Reparaz, M. R. Wagner, R. Kirste, C. Nenstiel, A. Hoffmann, and M. R. Phillips, Appl. Phys. Lett. **98**, 061906 (2011).
[33] S. G. Koch, E. V. Lavrov, and J. Weber (unpublished).
[34] C. B. Harris, R. M. Shelby, and P. A. Cornelius, Phys. Rev. Lett. **38**, 1415 (1977).
[35] B. N. J. Persson and R. Ryberg, Phys. Rev. B **32**, 3586 (1985).
[36] G. Lüpke, X. Zhang, B. Sun, A. Fraser, N. H. Tolk, and L. C. Feldman, Phys. Rev. Lett. **88**, 135501 (2002).
[37] K. R. Martin, P. Blaney, G. Shi, M. Stavola, and W. B. Fowler, Phys. Rev. B **73**, 235209 (2006).
[38] D. West and S. K. Estreicher, Phys. Rev. Lett. **96**, 115504 (2006).
[39] D. E. McCumber and M. D. Sturge, J. Appl. Phys. **34**, 1682 (1963).
[40] R. Elliott, W. Hayes, G. D. Jones, H. F. MacDonald, and C. T. Sennett, Proc. R. Soc. London, Ser. A **289**, 1 (1965).
[41] W. Ulrici and B. Clerjaud, Phys. Rev. B **70**, 205214 (2004).
[42] E. V. Lavrov, J. Weber, and F. Börrnert, Phys. Rev. B **77**, 155209 (2008).
[43] This point was brought to our attention during the review process. The referee is acknowledged for this constructive comment.
[44] U. Fano, Phys. Rev. **124**, 1866 (1961).
[45] A. Hewat, Solid State Commun. **8**, 187 (1970).
[46] J. Serrano, A. H. Romero, F. J. Manjón, R. Lauck, M. Cardona, and A. Rubio, Phys. Rev. B **69**, 094306 (2004).
[47] F. J. Manjón, B. Marí, J. Serrano, and A. H. Romero, J. Appl. Phys. **97**, 053516 (2005).
[48] J. Serrano, F. J. Manjón, A. H. Romero, A. Ivanov, M. Cardona, R. Lauck, A. Bosak, and M. Krisch, Phys. Rev. B **81**, 174304 (2010).
[49] K. Samanta, P. Bhattacharya, and R. S. Katiyar, J. Appl. Phys. **108**, 113501 (2010).
[50] A. Kaschner, U. Haboeck, M. Strassburg, M. Strassburg, G. Kaczmarczyk, A. Hoffmann, C. Thomsen, A. Zeuner, H. R. Alves, D. M. Hofmann, and B. K. Meyer, Appl. Phys. Lett. **80**, 1909 (2002).
[51] J. B. Wang, H. M. Zhong, Z. F. Li, and W. Lu, Appl. Phys. Lett. **88**, 101913 (2006).
[52] F. Friedrich and N. H. Nickel, Appl. Phys. Lett. **91**, 111903 (2007).
[53] X. Zhu, H. Wu, Z. Yuan, J. Kong, and W. Shen, J. Raman Spectrosc. **40**, 2155 (2009).
[54] F. Friedrich, M. A. Gluba, and N. H. Nickel, Appl. Phys. Lett. **95**, 141903 (2009).
[55] K. Wu, Q. Fang, W. Wang, M. A. Thomas, and J. Cui, J. Appl. Phys. **111**, 063530 (2012).
[56] C. A. Arguello, D. L. Rousseau, and S. P. S. Porto, Phys. Rev. **181**, 1351 (1969).
[57] F. Herklotz, E. V. Lavrov, and J. Weber, Phys. B (Amsterdam) **404**, 4349 (2009).
[58] J. K. Park, K. W. Lee, and C. E. Lee, Appl. Phys. Lett. **103**, 023109 (2013).
[59] G. A. Shi, M. Saboktakin, M. Stavola, and S. J. Pearton, Appl. Phys. Lett. **85**, 5601 (2004).
[60] M. D. McCluskey, S. J. Jokela, K. K. Zhuravlev, P. J. Simpson, and K. G. Lynn, Appl. Phys. Lett. **81**, 3807 (2002).
[61] E. V. Lavrov, F. Herklotz, and J. Weber, Phys. Rev. Lett. **102**, 185502 (2009).